The Distance-Based Eighth-Degree Closure Polynomial for the FANUC CRX Robot Series

Federico Thomas and Josep M. Porta

Abstract The FANUC CRX series of collaborative robots features a kinematic architecture in which every pair of adjacent joint axes is coplanar, intersecting at either a proper or improper point. While simpler to manufacture than conventional wrist-partitioned designs, this joint arrangement complicates kinematic analysis. In this paper, we show that its distance-based closure equation is a polynomial of degree eight, contrary to what happens with standard formulations which lead to polynomials of degree sixteen. Moreover, this polynomial is surprisingly tractable: its coefficients can be derived in compact, fully symbolic form.

1 Introduction

The kinematic architecture of collaborative robots (cobots) represents a deliberate departure from traditional industrial manipulators. Whereas conventional industrial robots employ partitioned, spherical-wrist designs optimized for speed and precision in isolated workspaces, cobots prioritize intrinsic safety and flexible human-robot collaboration. This shift is typically achieved through simplified mechanical designs featuring offset joints, transferring inherent kinematic complexity to the software layer for tasks such as inverse kinematics resolution and singularity management. Consequently, a fundamental compromise has become widely accepted in cobot

---

F. Thomas
Institut de Robòtica i Informàtica Industrial (CSIC-UPC), ETSEIB, Diagonal 647, Pavelló E
08028 Barcelona, Spain
e-mail: f.thomas@csic.es

J. M. Porta
Institut de Robòtica i Informàtica Industrial (CSIC-UPC), ETSEIB, Diagonal 647, Pavelló E
08028 Barcelona, Spain
e-mail: porta@iri.upc.edu

design: trading computational efficiency and autonomous operation for safety and collaborative flexibility.

This paper challenges the universality of this trade-off. We demonstrate that a prominent family of cobots —exemplified by the FANUC CRX series and its kinematic analogues— possesses a particular joint arrangement that simultaneously enables collaborative safety and preserves kinematic efficiency. As shown in Fig. 1, the FANUC CRX series employs a distinctive geometry where all consecutive joint axes are coplanar, with adjacent axes intersecting at finite points except for one parallel pair intersecting at infinity.

By exploiting this specific geometry in a distance-based formulation, this paper shows that, despite the robot's potential for up to sixteen real inverse kinematic solutions —consistent with general 6R manipulators— its distance-based closure polynomial reduces to degree eight. The derivation of this polynomial is remarkably concise, implementable in just a few lines of code in software languages such as MATLAB.

Previous work on the FANUC CRX-10iA/L has approached the closure polynomial from different perspectives. Carbonari et al. [1] obtained a 16-degree polynomial through scalar equation formulation and variable elimination, confirming the maximum theoretical number of IK solutions. Salunkhe et al. [2] applied the general algorithm of Husty et al. [3], also yielding a 16-degree polynomial, though their method required recomputation for each base-hand transformation and could not capture solutions with joint angles equal to π due to half-angle tangent substitutions. More recently, Thomas et al. [4, 5] introduced a distance-based formulation producing an 8-degree polynomial whose roots correspond one-to-two with the 16 workspace solutions. This paper presents a simplified version of this latter approach that yields the 8-degree polynomial in generic form through straightforward algebraic manipulation.

The remainder of this paper is structured as follows. Section 2 introduces the essential mathematical background. Section 3 reformulates the inverse kinematics of the FANUC CRX-10iA/L as a distance geometry problem. Based on this formulation, an example is presented in Section 4. The main contributions are summarized in Section 5.

2 Cayley-Menger Bideterminants and Their Derivatives

The Cayley-Menger bideterminant generalizes the classical Cayley-Menger determinant to partitions of point sets [6]. Given $2n$ points $P_1, \ldots, P_{2n}$ in a Euclidean space with squared distances $s_{ij} = \|P_i - P_j\|^2$, the bideterminant for the partition $(1 \ldots n \mid n+1 \ldots 2n)$ is defined as the $(n+1) \times (n+1)$ determinant:

$$\Phi\begin{pmatrix} 1 & \dots & n \\ n+1 & \dots & 2n \end{pmatrix} = \begin{vmatrix} 0 & 1 & 1 & \dots & 1 \\ 1 & s_{1,n+1} & s_{1,n+2} & \dots & s_{1,2n} \\ 1 & s_{2,n+1} & s_{2,n+2} & \dots & s_{2,2n} \\ \vdots & \vdots & \vdots & \ddots & \vdots \\ 1 & s_{n,n+1} & s_{n,n+2} & \dots & s_{n,2n} \end{vmatrix}. \tag{1}$$

This determinant has a direct geometric interpretation because it can be proved that

$$\Phi\begin{pmatrix} 1 \dots n \\ n+1 \dots 2n \end{pmatrix} \propto V_{1,2,\dots,n}\ V_{n+1,n+2,\dots,2n}, \tag{2}$$

where $V_{i_1,\dots,i_{k+1}}$ denotes the oriented k-dimensional volume of the simplex formed by the indicated points. The order of indices matters due to orientation.

When $P_i = P_{i+n}$ for $1 \le i \le n$, the bideterminant reduces to the ordinary Cayley-Menger determinant $\Phi(1 \dots n)$, which satisfies

$$\Phi(1 \dots n) \propto \left(V_{1,2,\dots,n}\right)^2. \tag{3}$$

Consequently, in $\mathbb{R}^3$, any Cayley-Menger bideterminant involving more than eight points —or any ordinary Cayley-Menger determinant involving more than four points— vanishes identically.

The derivative of a bideterminant with respect to $s_{i,j}$ (where $1 \le i \le n$ and $n+1 \le j \le 2n$) equals the corresponding cofactor (including its sign). For instance:

$$\frac{\partial}{\partial s_{2,5}}\Phi\begin{pmatrix} 1 & 2 & 3 \\ 4 & 5 & 6 \end{pmatrix} = -\Phi\begin{pmatrix} 1 & 3 \\ 4 & 6 \end{pmatrix}. \tag{4}$$

When some points appear in both partitions, the derivative must account for all occurrences of $s_{i,j}$ in the determinant. Thus, it equals the sum of the corresponding cofactors. For example:

$$\frac{\partial}{\partial s_{2,5}}\Phi\begin{pmatrix} 1 & 2 & 5 \\ 4 & 5 & 2 \end{pmatrix} = \Phi\begin{pmatrix} 1 & 5 \\ 4 & 2 \end{pmatrix} + \Phi\begin{pmatrix} 1 & 2 \\ 4 & 5 \end{pmatrix}. \tag{5}$$

For ordinary Cayley-Menger determinants, the derivative with respect to $s_{i,j}$ (where $1 \le i, j \le n$) is twice the cofactor of $s_{i,j}$ (equivalently $s_{j,i}$), as each point appears in both row and column sets. For example:

$$\frac{\partial}{\partial s_{1,3}}\Phi(1,2,3) = 2\,\Phi\begin{pmatrix} 2 & 3 \\ 1 & 2 \end{pmatrix} = 2\,\Phi\begin{pmatrix} 1 & 2 \\ 2 & 3 \end{pmatrix}. \tag{6}$$

3 Distance-Based Formulation and Closure Polynomial

The kinematic structure of the FANUC CRX-10iA/L can be modeled as the bar-and-joint framework shown in Fig. 2(left). Here, $P_2, P^\infty, P_4, P_5, P_6$ correspond to

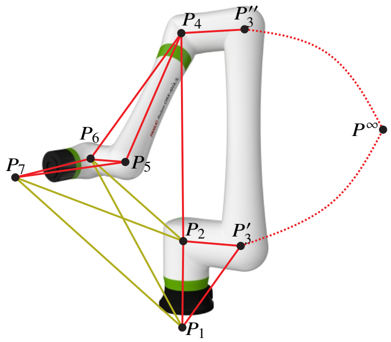

Link (i)	d_i (mm)	a_i (mm)	α_i (rad)
1	245	0	$\pi/2$
2	260	710	0
3	-260	0	$-\pi/2$
4	540	0	$\pi/2$
5	150	0	$\pi/2$
6	160	0	0

	P_1	P_2	P_4	P_5	P_6	P_7
P_1	0	245^2				
P_2	245^2	0	710^2			
P_4		710^2	0	540^2	$540^2{+}150^2$	
P_5			540^2	0	150^2	
P_6			$540^2{+}150^2$	150^2	0	160^2
P_7					160^2	0

Fig. 1 Kinematic model and invariant distances of the FANUC CRX-10iA/L. Left: the robot's consecutive joint axes are coplanar, intersecting at finite points (P_2, P_4, P_5, P_6) except for the parallel axes 3 and 4, which intersect at the improper point P^∞. Right: table of its DH parameters and table of fixed squared distances (in mm^2) between these points.

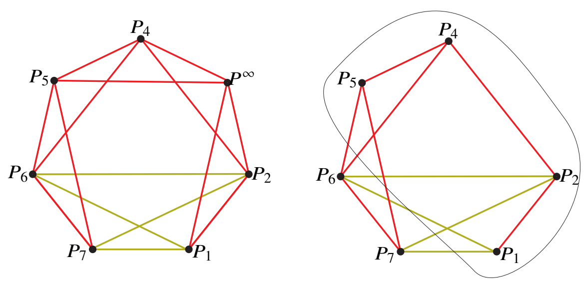

Fig. 2 Distance-based bar-and-joint framework. Left: distance graph modeling the FANUC CRX-10iA/L. Vertices correspond to points on the joint axes (see Fig. 1). Edges represent distance constraints: red bars have fixed lengths (link parameters); green bars have lengths determined by the desired end-effector pose. The improper point P^∞ models the intersection at infinity of parallel axes 3 and 4. Right: simplified six-point graph obtained by imposing the coplanarity condition $\Phi(1,2,4,5) = 0$, which eliminates P^∞. The four coplanar points are highlighted.

intersections of consecutive joint axes, while P_1 and P_7 may be chosen arbitrarily along the first and last axes (with $P_1 \neq P_2$ and $P_6 \neq P_7$).

Once the end-effector is fixed in a given pose with respect to the robot's base, the four points $\{P_1, P_2, P_6, P_7\}$ define a tetrahedron of known edge lengths and orientation. Thus, the inverse kinematics problem reduces to determining all valid three-dimensional realizations of this framework subject to its distance constraints. The improper point P^∞ can be eliminated by enforcing coplanarity of P_1, P_2, P_4, and P_5, yielding a simplified framework involving only six points (Fig. 2(right)).

Observe that any subset of five points in the framework of Fig. 2(a) defines a degenerate simplex in $\mathbb{R}^3$ with zero volume. Additionally, the simplex formed by $\{P_1, P_2, P_4, P_5\}$ has zero volume due to coplanarity. These constraints can be expressed via Cayley-Menger determinants involving five points. With six points and eleven specified pairwise distances, we obtain six equations —plus the equation derived from the coplanarity constraint— in four unknowns. While these redundant representations could be exploited when using interval-based methods [7], a minimal formulation is preferable for deriving a univariate resultant polynomial. Minimal systems can be systematically obtained by decomposing the framework into tetrahedral strips [8, 9]. One such minimal system can be proved to be:

$$\Phi(1,2,5,6,7) = 0 \Rightarrow f_1(s_{2,5}, s_{1,5}) = 0 \tag{7}$$

$$\Phi(1,2,4,5) = 0 \Rightarrow f_2(s_{2,5}, s_{1,5}, s_{1,4}) = 0 \tag{8}$$

$$\Phi(1,2,4,5,6) = 0 \Rightarrow f_3(s_{2,5}, s_{1,5}, s_{1,4}) = 0 \tag{9}$$

This yields three algebraic equations in three unknowns $(s_{2,5}, s_{1,5}, s_{1,4})$ which are the squared distances between the points indicated by the subscripts. A key advantage of the tetrahedral strip decomposition is that it produces, for mechanisms with coupling number one, a cascade system where the first equation involves two variables, each subsequent equation introduces only one new variable relative to the previous ones, and the last equation introduces no new variables. This structured dependency simplifies the resultant computation through backward sequential variable elimination using dialytic elimination. This strategy has recently been proven to be simpler to implement and faster to execute than our previous radical-clearing approach [10].

A resultant for the above system can thus be obtained by first eliminating $s_{1,4}$ from (9) and (8), and then eliminating $s_{1,5}$ from the resulting expression and (7). The final result is an eighth-degree polynomial in $s_{2,5}$. This can be implemented in few lines of code. To the best of our knowledge, no other known method could attain this level of simplicity.

Although we could conclude our analysis at this point, it is instructive to examine the algebraic structure of this problem more closely —both to better appreciate the power of distance-based formulations and to explicitly derive the resultant. First, we apply the Desnanot-Jacobi identity to $\Phi(1,2,4,5,6)$, which gives:

$$\Phi(1,2,4,5,6)\Phi(2,4,5) = \Phi(1,2,4,5)\Phi(2,4,5,6) - \Phi^2\begin{pmatrix}1,2,4,5\\2,4,5,6\end{pmatrix}. \tag{10}$$

Since $\Phi(1,2,4,5,6) = 0$ (equation (9)) and $\Phi(1,2,4,5) = 0$ (equation (8)), we conclude that:

$$\Phi\begin{pmatrix}1,2,4,5\\2,4,5,6\end{pmatrix} = -\Phi\begin{pmatrix}2,4,5,1\\2,4,5,6\end{pmatrix} = 0. \tag{11}$$

This equation remains quadratic in $s_{2,5}$ but is linear in $s_{1,5}$ and $s_{1,4}$. Expanding it in terms of $s_{1,4}$ yields:

$$\Phi\begin{pmatrix}2,4,5,1\\2,4,5,6\end{pmatrix} = \Phi\begin{pmatrix}2,5,4\\2,5,6\end{pmatrix} s_{1,4} + \Phi\begin{pmatrix}2,4,5,1\\2,4,5,6\end{pmatrix}\Bigg|_{s_{1,4}=0} = 0. \tag{12}$$

Similarly, expanding equation (8) in terms of $s_{1,4}$ via derivatives yields:

$$\Phi(1,2,4,5) = \Phi(2,5)s_{1,4}^2 + 2\Phi\begin{pmatrix}2,4,5\\1,2,5\end{pmatrix}\Bigg|_{s_{1,4}=0} s_{1,4} + \Phi(1,2,4,5)|_{s_{1,4}=0} = 0. \tag{13}$$

Solving (12) for $s_{1,4}$ and substituting into (13) leads to $CB^2 - 2DAB + EA^2 = 0$, where A and C are independent of $s_{1,5}$; B and D are linear in $s_{1,5}$; and E is quadratic in $s_{1,5}$. Therefore,

$$CB^2 - 2DAB + EA^2 = \alpha_2 s_{1,5}^2 + \alpha_1 s_{1,5} + \alpha_0 = 0. \tag{14}$$

Similarly, expanding equation (7) in terms of $s_{1,5}$ yields:

$$\beta_2 s_{1,5}^2 + \beta_1 s_{1,5} + \beta_0 = 0. \tag{15}$$

Finally, eliminating $s_{1,5}$ from (14) and (15) via Sylvester dialytic elimination gives the resultant:

$$\begin{vmatrix} \alpha_2 & \alpha_1 & \alpha_0 & 0 \\ 0 & \alpha_2 & \alpha_1 & \alpha_0 \\ \beta_2 & \beta_1 & \beta_0 & 0 \\ 0 & \beta_2 & \beta_1 & \beta_0 \end{vmatrix} = 0. \tag{16}$$

It can be seen that this resultant is an eighth-degree polynomial in $s_{2,5}$. Explicit expressions for all coefficients above are omitted due to space constraints.

4 Example

With the base and end-effector fixed, we assign coordinates $(0, 0, 0)$, $(0, 0, 0.245)$, $(-0.4, 0, 0.16)$, and $(-0.4, 0, 0)$ to points P_1, P_2, P_6, and P_7, respectively. Then, substituting all known distances into (16) leads to the following eighth-degree closure polynomial:

$$\begin{aligned} &s_{2,5}^8 - 1.4289 s_{2,5}^7 + 0.87182 s_{2,5}^6 - 0.29725 s_{2,5}^5 + 0.062198 s_{2,5}^4 \\ &- 0.0081581 s_{2,5}^3 + 0.00065955 s_{2,5}^2 - 0.0000300534 s_{2,5} + 5.91824 \cdot 10^{-7} = 0. \end{aligned}$$

This eighth-degree polynomial equation has eight real roots that form three distinct numerical clusters. Within a tolerance of 10^{-9}, these clusters are centered at $s_{2,5}^a \approx 0.1207$ (two roots), $s_{2,5}^b \approx 0.144725$ (four roots), and $s_{2,5}^c \approx 0.3043$ (two roots). The corresponding configurations (4, 8, and 4 in each cluster) occur at singular poses. In particular, the cluster of four roots corresponds to a higher-order singularity where several singular conditions are satisfied.

With $s_{2,5}$ determined, backsubstitution yields $s_{1,4}$ and $s_{1,5}$. The Cartesian coordinates of P_5, P_4, P_3'', and P_3' are then computed from those of the fixed points P_1, P_2, P_6, and P_7 through the following sequence of geometric constructions: (1) trilateration of P_5 from its distances to P_2, P_6, and P_7 (two candidates); (2) constrained location of P_4 from its distances to P_2 and P_6, subject to the coplanarity condition $P_4 \in \text{plane}(P_2, P_6, P_7)$ (two candidates); (3) trilateration of P_3'' from its distances to P_2, P_4, and P_5 (two candidates); and (4) multilateration of P_3' from distances to P_1, P_2, P_4, and P_3'' (a unique candidate).

Thus, a single value of $s_{2,5}$ generates up to $2^3 = 8$ candidate configurations. While not all are physically feasible, a significant departure from prior distance-geometry applications occurs: here, each root of the 8th-degree closure polynomial yields two feasible inverse kinematic solutions, rather than the usual one-to-one correspondence. This doubling explains why the robot can admit up to 16 real configurations despite the polynomial's lower degree —a structural feature inherent to its geometry.

A rigorous justification stems from the fact that a distance matrix can be coordinatized uniquely up to isometries —rotations, translations, and reflections. Since the tetrahedron $P_1P_2P_3P_4$ is fixed (and hence oriented), the complete set of squared pairwise distances s_{ij} among all points $P_1, \ldots, P_7$ uniquely determines the robot configuration, for example, via Cholesky factorization. Therefore, for a given triple $(s_{2,5}, s_{1,4}, s_{1,5})$ together with the known fixed distances, the distance matrix must admit exactly two distinct completions. This mathematically explains the observed doubling of feasible configurations for each polynomial root.

The Cartesian coordinates of P_5, P_4, P''_3, and P'_3 for all 16 solutions are listed in Table I. Each solution is identified with a sign triplet corresponding to the branch selections described earlier. As expected, each triplet appears twice, confirming the one-to-two mapping between polynomial roots and configurations. Fig. 3 provides a schematic orthographic representation of all configurations from the same arbitrary viewpoint.

Table I Cartesian coordinates (in meters) for the 16 inverse kinematic solutions. Solutions are listed with their corresponding sign triplet from the geometric construction sequence described in Section 5.

	1 $(-+-)$	**2** $(-++)$	**3** $(+--)$	**4** $(+-+)$
$P_{3'}$	(-0.0947,0.2421,0.2450)	(0.0947,-0.2421,0.2450)	(0.0947,0.2421,0.2450)	(-0.0947,-0.2421,0.2450)
$P_{3''}$	(-0.4084,0.1194,-0.3800)	(-0.2190,-0.3648,-0.3800)	(-0.2190,0.3648,-0.3800)	(-0.4084,-0.1194,-0.3800)
P_4	(-0.3137,-0.1227,-0.3800)	(-0.3137,-0.1227,-0.3800)	(-0.3137,0.1227,-0.3800)	(-0.3137,0.1227,-0.3800)
P_5	(-0.3137,-0.1227,0.1600)	(-0.3137,-0.1227,0.1600)	(-0.3137,0.1227,0.1600)	(-0.3137,0.1227,0.1600)
	5 $(---)$	**6** $(--+)$	**7** $(-+-)$	**8** $(-++)$
$P_{3'}$	(0.0975,-0.2410,0.2450)	(-0.0975,0.2410,0.2450)	(-0.0975,0.2410,0.2450)	(0.0975,-0.2410,0.2450)
$P_{3''}$	(-0.4371,-0.4573,0.6592)	(-0.6321,0.0248,0.6592)	(-0.4114,0.1140,-0.3790)	(-0.2164,-0.3680,-0.3790)
P_4	(-0.5346,-0.2162,0.6592)	(-0.5346,-0.2162,0.6592)	(-0.3139,-0.1270,-0.3790)	(-0.3139,-0.1270,-0.3790)
P_5	(-0.3438,-0.1391,0.1600)	(-0.3438,-0.1391,0.1600)	(-0.3438,-0.1391,0.1600)	(-0.3438,-0.1391,0.1600)
	9 $(+--)$	**10** $(+-+)$	**11** $(++-)$	**12** $(+++)$
$P_{3'}$	(0.0975,0.2410,0.2450)	(-0.0975,-0.2410,0.2450)	(-0.0975,-0.2410,0.2450)	(0.0975,0.2410,0.2450)
$P_{3''}$	(-0.2164,0.3680,-0.3790)	(-0.4114,-0.1140,-0.3790)	(-0.6321,-0.0248,0.6592)	(-0.4371,0.4573,0.6592)
P_4	(-0.3139,0.1270,-0.3790)	(-0.3139,0.1270,-0.3790)	(-0.5346,0.2162,0.6592)	(-0.5346,0.2162,0.6592)
P_5	(-0.3438,0.1391,0.1600)	(-0.3438,0.1391,0.1600)	(-0.3438,0.1391,0.1600)	(-0.3438,0.1391,0.1600)
	13 $(---)$	**14** $(--+)$	**15** $(++-)$	**16** $(+++)$
$P_{3'}$	(0.0213,-0.2591,0.2450)	(-0.0213,0.2591,0.2450)	(-0.0213,-0.2591,0.2450)	(0.0213,0.2591,0.2450)
$P_{3''}$	(-0.5219,-0.3037,0.7000)	(-0.5645,0.2145,0.7000)	(-0.5645,-0.2145,0.7000)	(-0.5219,0.3037,0.7000)
P_4	(-0.5432,-0.0446,0.7000)	(-0.5432,-0.0446,0.7000)	(-0.5432,0.0446,0.7000)	(-0.5432,0.0446,0.7000)
P_5	(-0.5432,-0.0446,0.1600)	(-0.5432,-0.0446,0.1600)	(-0.5432,0.0446,0.1600)	(-0.5432,0.0446,0.1600)

In every one of the 16 configurations, a privileged projection axis exists that is parallel to the three joint-axis planes (represented by the green, blue, and red

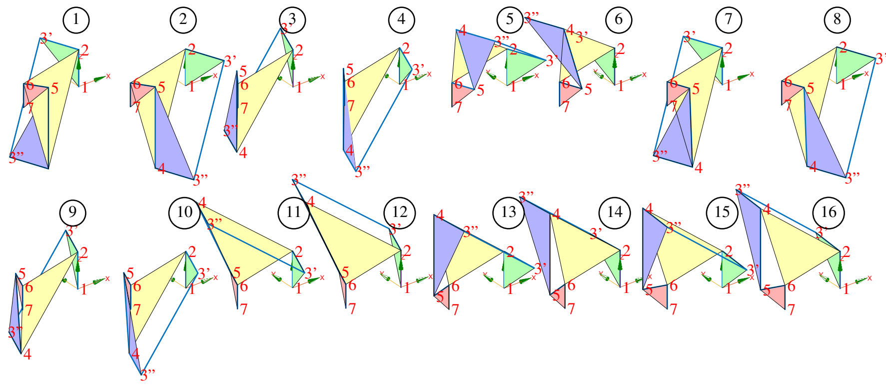

Fig. 3 The 16 inverse kinematic configurations. Schematic orthographic view (from an arbitrary viewpoint) of all real solutions for the end-effector pose given in Section 5. Configurations are numbered 1-16 as in Table I. The triangles highlight the three planes defined by consecutive joint axes: the base plane $P_1P_2P_{3'}$ (green), the middle plane $P_{3''}P_4P_5$ (blue, defined by the parallel axes), and the end-effector plane $P_5P_6P_7$ (red). The yellow triangle $P_2P_4P_6$ is included for spatial reference.

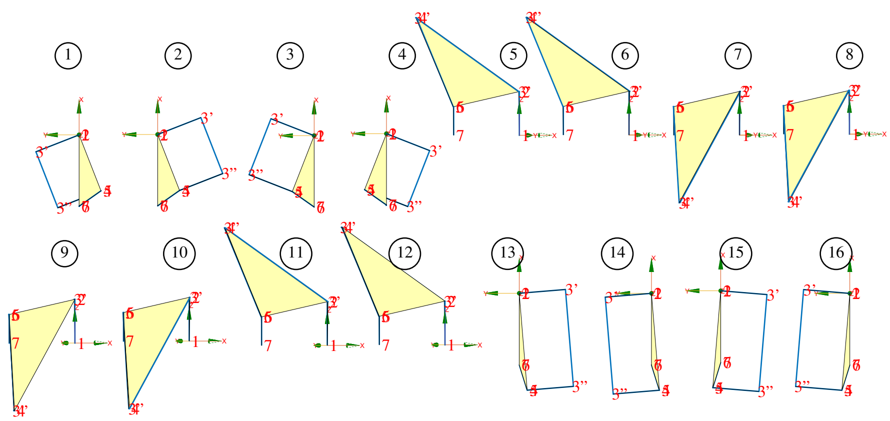

Fig. 4 Singular nature of all 16 configurations. Each configuration is shown from a viewing axis parallel to its three joint-axis planes (green, blue, red). In this projection, those planes appear as lines, visually confirming their parallelism —a condition that corresponds to a kinematic singularity. The yellow triangle $P_2P_4P_6$ remains visible as a non-degenerate reference. For the configurations corresponding to the cluster of four roots (e.g., configurations 5-12), the blue and red planes are also coplanar, indicating a higher-order singularity.

triangles), confirming that all configurations are singular. For the eight configurations from the four-root cluster, the blue and red triangles are additionally coplanar, signifying a higher-order singularity. Fig. 4 shows all configurations using such a parallel projection where only the yellow triangle remains visible —the other three triangles appear as lines because they are parallel to the viewing axis.

5 Concluding Remarks

We have shown that the inverse kinematics of the FANUC CRX robot series reduces to finding the roots of an eighth-degree polynomial, a result enabled by its unique kinematic geometry. By employing a distance-based formulation and representing the manipulator as a bar-and-joint framework, we derived this polynomial through a cascade of two elementary variable eliminations. This derivation is remarkably simpler than previous approaches yielding polynomials of degree sixteen.

Acknowledgements This work was partially supported by the Spanish Ministry of Science through project PID2024-161798NB-100 (MCIU/AEI/10.13039/501100011033 and ERDF/UE).

References

1. L. Carbonari, M.-C. Palpacelli, M. Callegari, Inverse kinematics of a class of 6R collaborative robots with non-spherical wrist, *Robotics* 12 (2) (2023) 36.
2. D. H. Salunkhe, Robots cuspidaux: étude théorique, classification et applications aux robots commerciaux (title in French, but text in English), Phd dissertation, École Centrale de Nantes (2023).
3. M. L. Husty, M. Pfurner, H.-P. Schröcker, A new and efficient algorithm for the inverse kinematics of a general serial 6R manipulator, *Mechanism and Machine Theory* 42 (1) (2007) 66–81.
4. F. Thomas and J. M. Porta, The distance geometry of the generalized lobster's arm, in *Advances in Robot Kinematics*, Vol. 24, Springer, 2022, pp. 409–417.
5. F. Thomas and J. M. Porta, The inverse kinematics of lobster arms, *Mechanism and Machine Theory* 196 (2024) 105630.
6. L. Blumenthal, Theory and Applications of Distance Geometry. Oxford, U.K.: Oxford Univ. Press, 1953.
7. J. M. Porta, L. Ros, F. Thomas, and C. Torras, A Branch-and-Prune solver for distance constraints, *IEEE Transactions on Robotics* 21 (2) (2005) 176–187.
8. F. Thomas and J. M. Porta, Closure polynomials for strips of tetrahedra, in *Advances in Robot Kinematics*, Springer, 2016, pp. 303–312.
9. J. M. Porta and F. Thomas, The forward kinematics of doubly-planar Gough-Stewart platforms and the position analysis of strips of tetrahedra, in *Advances in Robot Kinematics*, Springer, 2018.
10. J. M. Porta and F. Thomas, Yet another approach to the Gough-Stewart platform forward kinematics, *Proc. of the IEEE International Conference in Robotics and Automation*, 2018.